

Journal of Biomedical Optics

SPIEDigitalLibrary.org/jbo

Porcine cortical bone ablation by ultrashort pulsed laser irradiation

Brent Emigh
Ran An
Eugene M. Hsu
Travis H. R. Crawford
Harold K. Haugen
Gregory R. Wohl
Joseph E. Hayward
Qiyin Fang

Porcine cortical bone ablation by ultrashort pulsed laser irradiation

Brent Emigh,^a Ran An,^b Eugene M. Hsu,^b Travis H. R. Crawford,^b Harold K. Haugen,^c Gregory R. Wohl,^d Joseph E. Hayward,^a and Qiyin Fang^e

^aMcMaster University, Department of Medical Physics and Applied Radiation Sciences, 1280 Main Street West, Hamilton, Ontario, Canada L8S 4K1

^bMcMaster University, Department of Engineering Physics, 1280 Main Street West, Hamilton, Ontario, Canada L8S 4K1

^cMcMaster University, Department of Engineering Physics, and Department of Physics and Astronomy, 1280 Main Street West, Hamilton, Ontario, Canada L8S 4K1

^dMcMaster University, Department of Mechanical Engineering, and School of Biomedical Engineering, 1280 Main Street West, Hamilton, Ontario, Canada L8S 4K1

^eMcMaster University, Department of Engineering Physics, and School of Biomedical Engineering, 1280 Main Street West, Hamilton, Ontario, Canada L8S 4K1

Abstract. Ultrashort pulsed lasers in bone ablation show promise for many orthopedic applications. To minimize collateral tissue damage and control the ablation process, the ablation threshold fluence must be well characterized. Using an amplified femtosecond laser (170 fs, 800 nm, 1 kHz), the ablation threshold on unaltered porcine cortical bone was measured using the D^2 method at multiple incident pulse numbers ranging from 25 to 1000 pulses per spot. The lowered threshold at greater pulse numbers indicated an incubation effect. Using a power law model, the incubation coefficient of unaltered porcine cortical bone was found to be 0.89 ± 0.03 . Through extrapolation, the single-pulse ablation threshold was found to be $3.29 \pm 0.14 \text{ J/cm}^2$. © 2012 Society of Photo-Optical Instrumentation Engineers (SPIE). [DOI: 10.1117/1.JBO.17.2.028001]

Keywords: laser ablation; orthopedic applications.

Paper 11479 received Sep. 3, 2011; revised manuscript received Dec. 15, 2011; accepted for publication Dec. 19, 2011; published online Feb. 27, 2012.

1 Introduction

It has been demonstrated that lasers may be used to cut or drill bone tissue for orthopedic surgical applications.¹⁻³ Compared to the mechanical drill or saw, laser ablation has a number of potential advantages, including minimal mechanical vibration, the ability to focus to small spot size, no direct target contact, and the ability to integrate with real-time optical sensing. These advantages allow for an intricate cut geometry as well as precise control with real-time feedback. Recent work with ultrashort pulsed lasers (pulse durations <10 ps) has produced highly efficient ablation (i.e., small laser energy input per ablated volume of tissue) in bone while resulting in only minimal collateral damage.⁴⁻⁷ At sufficiently high irradiances, the ablation process is a direct solid-plasma transition,⁸ which explains the aforementioned benefits of ultrashort laser pulses. The high instantaneous peak power induces nonlinear absorption and subsequent tissue removal while the low average power deposited during ultrashort laser ablation results in minimal thermal buildup. Due to the avoidance of cumulative thermal effects with ultrashort pulsed lasers for bone ablation, the chemical properties of hydroxyapatite, the main component of bone mineral, are preserved at the ablation site.⁹

The ablation threshold is the minimum laser fluence required to initiate substantial material removal from a surface. Using polished porcine cortical bone, Girard et al. found the ablation threshold to be 0.69 J/cm^2 when irradiated with 1000 pulses at

775 nm, a repetition rate of 1 kHz, and a pulse duration of 200 fs, but did not investigate the threshold with different pulse numbers.⁶ It has been reported that material surfaces, such as metals^{10,11} and semiconductors,¹² become damaged at fluences below the single-pulse ablation threshold when irradiated with multiple pulses. This phenomenon is referred to as the incubation effect. Described using a power law model,¹³ the incubation coefficient, ξ , characterizes the degree of this effect and is an intrinsic property of the material. Using laser pulses at 775 nm, a repetition rate of 3 kHz, and a pulse duration of 150 fs, Lim et al. conducted single-pulse ablation and linear scanned ablation tests to measure the single-pulse ablation threshold and incubation coefficient in polished bovine cortical bone.¹⁴ From their results, the authors calculated the ablation threshold at 1000 pulses per spot to be $1.22 \pm 0.29 \text{ J/cm}^2$. The difference in the reported ablation threshold values may be attributed to differences in the samples (e.g., porcine versus bovine, moisture, etc.) and the experimental design (e.g., single-pulse versus multiple-pulse ablation).

In both studies, the surfaces of the cortical bone samples were polished to achieve a uniformly flat and smooth ablation surface. Laser ablation strongly depends on the material composition and properties of the sample. In the context of investigating ablation thresholds, a polished bone surface may differ considerably from the natural cortical bone surface. For example, sanding the bone surface can increase specular reflection, while surface corrugations can change the local field intensity and affect the threshold fluence.¹⁵ Therefore, it is also important to investigate the ablation threshold using unaltered bone samples.

Address all correspondence to: Qiyin Fang, McMaster University, Department of Engineering Physics, and School of Biomedical Engineering, 1280 Main Street West, Hamilton, Ontario, Canada L8S 4K1. Tel: 9055259140; E-mail: qiyin.fang@mcmaster.ca.

Laser machining of bone during surgical procedures requires a large number of laser pulses. Therefore, characterizing the incubation effect from multiple pulses would have important implications in determining the optimum ablation parameters. In this study, we used a varying number of pulses to obtain the single-pulse ablation threshold. The incubation effect in unpolished porcine cortical bone was quantified through the measurement of the incubation coefficient.

2 Methods

2.1 Ablation Experimental Setup

The ablation experiments were performed using a customized ultrafast laser machining system whose schematic is shown in Fig. 1, which was similar to the setup used in our previous work.¹⁶ Briefly, a Ti:Sapphire mode-locked oscillator (Tsunami, Spectra Physics) seeded a chirped-pulse amplifier (Spitfire, Spectra Physics) to generate laser pulses at $\sim 325 \mu\text{J}$ and 170 fs [full width half maximum (FWHM)], which was measured using a second-order noncollinear autocorrelator. For all experiments in this report, a 1 kHz repetition rate and 800 nm wavelength output were used and the peak wavelength was verified by a fiber-coupled spectrometer (PC2000, Ocean Optics). The collimated beam was reduced in diameter through the use of a telescope and had a final $1/e^2$ diameter of 4.42 mm. The beam had a near Gaussian intensity profile that was measured using a laser beam profiler (BeamStar, Ophir Optonics). The pulse energy was controlled using a set of neutral density filters. A small portion of the laser beam was reflected onto a calibrated photodiode (DET210, ThorLabs) that monitored the laser energy after passing through the filters. The laser exposure time (i.e., number of pulses delivered to the sample) was adjusted by a computer-controlled mechanical shutter (VS25S2S1, Uniblitz). Beyond the shutter, the beam was steered into a plano-convex lens ($f = 12.5 \text{ cm}$, BK7), which focused the collimated beam down to a $1/e^2$ spot size diameter of $30.2 \mu\text{m}$.

The spot size was confirmed by measurement in preliminary experiments using the same focusing scheme to avoid potential

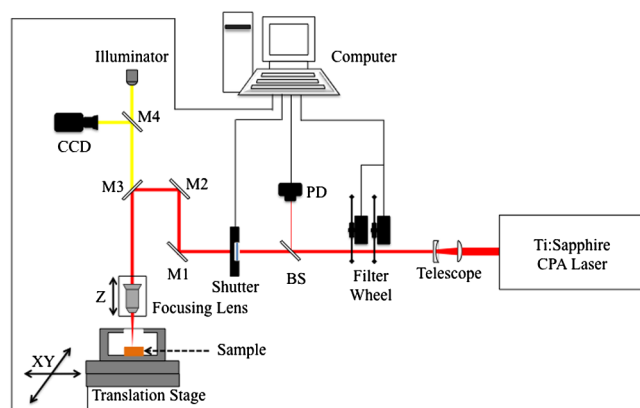


Fig. 1 Schematics of the laser ablation setup. After exiting the chirped-pulse amplifier (CPA), the beam energy was adjusted with a set of two computer-controlled filter wheels. A beam splitter (BS) picked off a portion of the beam and directed it onto a calibrated photodiode (PD). The signal from the PD was sent to a box-car integrator (not shown), whose output was read out by the computer. The shutter was computer controlled. The CCD camera monitored the ablation process to ensure laser—sample alignment. M1 and M2 are high reflection mirrors. M3 is a dichroic mirror, and M4 is a beam splitter.

errors caused by the rough bone surface. Using a piece of silicon as the target, the laser focusing plane was found by iteratively reducing the laser power and moving the lens along the optical axis. The lens position was found where ablation of silicon occurred, while a small change of the lens position caused ablation to no longer occur. As shown in Fig. 1, the target was imaged to the CCD through both the laser focusing lens and another lens in front of the CCD. After the laser focusing plane was located, the focusing lens in front of the CCD was adjusted to give this position a sharp image on the camera display. These steps assured the laser focusing and the CCD imaging planes were the same and images of the target were collimated between the two lenses before focusing on the CCD. Before each ablation experiment, the focusing lens was adjusted on its translational stage until the image of the bone surface on the camera display appeared to be in sharp focus, which meant the laser also focused on the bone surface. Using a 125-mm focusing lens, there is a $200\text{-}\mu\text{m}$ range in which the sharpness of the bone surface appears to remain at a maximum. Assuming Gaussian beam propagation, a translational uncertainty of $200 \mu\text{m}$ in locating the laser focus on the sample in the viewing camera and a $1/e^2$ spot size diameter of $30.2 \mu\text{m}$ would result in a beam waist uncertainty of $0.74 \mu\text{m}$ and subsequent uncertainty in the fluence calculation.¹⁶

The bone sample was irradiated within a chamber mounted on a computer-controlled X-Y translational stage (UTM100PP.1, Newport). The focusing lens was mounted on a Z translation stage (MFN25PP, Newport) independent of the X-Y stage. A confocal monochrome CCD camera and white LED illuminator were used to monitor the sample alignment and the ablation process during the course of the experiments. The laser beam focal plane and CCD imaging focal plane were aligned before commencing each experiment.

2.2 Bone Samples

The experimental protocol was approved by the McMaster Animal Research Ethics Board. Bone specimens were harvested from the scapulae of skeletally immature pigs obtained from a local butcher. After harvesting, soft tissue and periosteum were cleaned off the specimens, which were then cut to include both the outer cortical layer (thicknesses 1 to 3 mm) as well as cancellous bone ($\sim 5 \text{ mm}$). In all ablation experiments, the laser beam was directed onto the surface of the cortical layer through a quartz cover glass slide inside a sealed glass chamber. The surface of the bone was left unaltered to mimic real-life conditions. All ablation experiments were performed within 24 h of harvesting. Following ablation, specimens were fixed in 10% formalin and stored in saline until further processing.

2.3 Ablation Procedure

Surface craters were ablated in bone with 25, 50, 75, 100, 300, 500, and 1000 incident pulses. Crater ablation was repeated over a range of 30 fluence levels from 0.1 to 13.0 J/cm^2 . This procedure was repeated three times on bone specimens from the scapulae of three different pigs. The craters were viewed using reflected-light microscopy (Axioplan 2, Zeiss), and crater diameters were measured using image analysis software (Northern Eclipse, Empix Imaging). The crater diameter was defined as the maximum diameter of the region of removed tissue. The D^2 technique,¹⁷ where the diameter of the ablated crater is correlated to the known laser energy used for that specific crater,

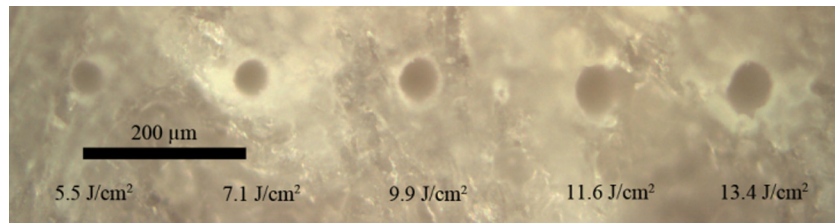


Fig. 2 Ablation craters cut into the surface of porcine cortical bone with 1000 pulses per spot at five different fluence levels. Imaged using a reflected-light optical microscope and a 20× objective.

was used to determine the threshold fluence for each incident pulse number. The relationship between the crater diameter and the peak laser fluence is given by:

$$D^2 = 2\omega_0^2 \ln\left(\frac{\phi}{\phi_{th}}\right), \quad (1)$$

where D is the diameter of removed tissue, ω_0 is the $1/e^2$ radius of the focused beam incident spot, ϕ is the fluence used for each crater, and ϕ_{th} is the threshold fluence for the sample. From the semilog plot of D^2 versus fluence, the ablation threshold can be determined from the x -intercept. The $1/e^2$ focal spot size can also be obtained from this plot and verified for consistency with previous investigations.

The incubation model of Jee et al.¹³ relates the fluence threshold for N pulses, $\phi_{th}(N)$, with the single-pulse ablation threshold, $\phi_{th}(1)$, and is given by:

$$\phi_{th}(N) = \phi_{th}(1) \times N^{\xi-1}, \quad (2)$$

where ξ is defined as the incubation coefficient. A rearrangement yields a logarithmic relationship between the accumulated fluence, $N \times \phi_{th}(N)$, and N , with the proportionality constant equal to ξ . A log–log plot of the accumulated fluence versus the incident pulse number will have a slope equal to the incubation coefficient and a y -intercept equal to the single-pulse ablation threshold.

3 Results

3.1 Ablation Threshold

An example of ablation craters in cortical bone after irradiation with 1000 pulses per spot is shown in Fig. 2. Using an optical microscope under 20× microscope viewing, orthogonal measurements of the diameter were carried out and the geometric average diameter was determined. Note that a small rim of discolored tissue surrounding each crater was observed and not taken into account when measuring the crater diameter (maximum diameter of removed tissue).

Squared diameter (D^2) versus log of the fluence plots were created for all incident pulse numbers. Exemplar plots (Fig. 3) are shown for 75 and 1000 incident pulses. The results from all three scapulae are plotted on the same figure as trials 1, 2, and 3. Scatter between trials was attributed to changes in bone surface topography and uncertainty in beam focus alignment. At fluences greater than 2 J/cm², the trend between squared diameter and fluence appeared to be logarithmic; however, craters ablated with fluence below 2 J/cm² appeared to follow a different trend.

Each individual trial was fit using a linear least-squares algorithm (not shown), and the weighted average slope and

y -intercept were calculated from the three trials and used to construct the trend lines shown in Fig. 3. From these lines, the energy fluence ablation thresholds were obtained for each incident pulse number and are shown in Table 1. Experimental

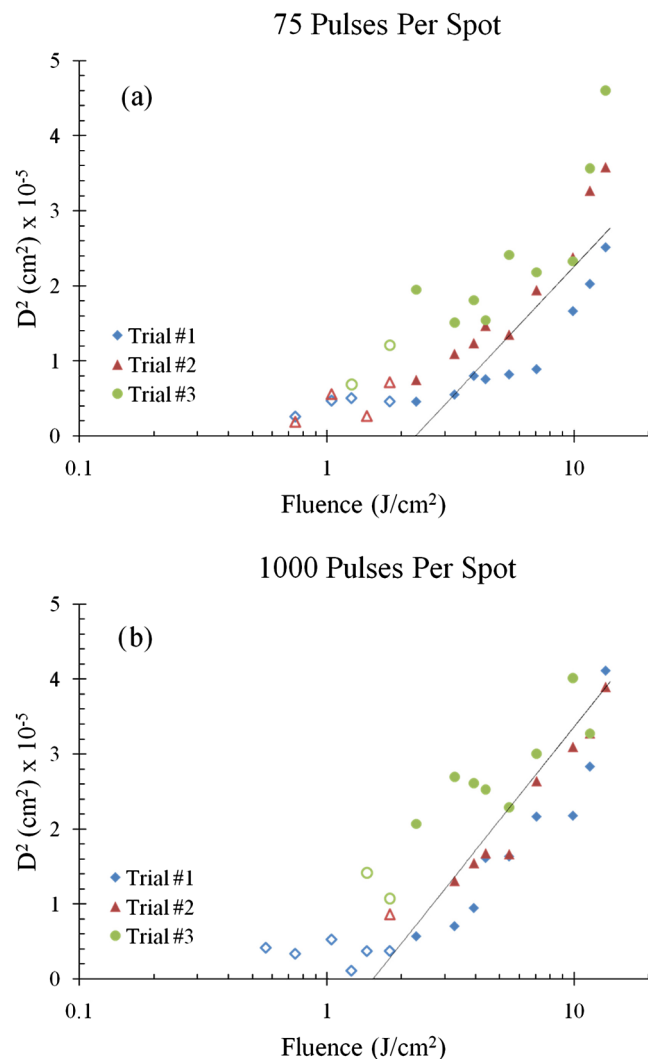


Fig. 3 Squared diameter (D^2) of ablated craters versus fluence in porcine cortical bone ablated by multiple pulses per spot: (a) 75 pulses per spot and (b) 1000 pulses per spot. Samples were irradiated with $\lambda = 800$ nm, $\tau = 170$ fs pulses at a repetition rate of 1 kHz. Three trials were performed on the scapular bones of individual pigs. Solid data points were assumed to be the result of a faster material-removal ablation regime and used in creating the lines of best fit. Hollow points indicate the results of an ablation regime with little material removal and were not included in the fit. The slope and intercept of the plotted trend line were obtained from the weighted average slope and intercept of the three individual trial least-squares lines.

Table 1 Ablation threshold fluence at different incident pulse numbers as measured using the D^2 method.^a

Incident pulse number (N)	Ablation threshold fluence (J/cm^2)
25	2.37 ± 0.78
50	2.36 ± 0.87
75	2.28 ± 0.76
100	1.72 ± 0.93
300	1.66 ± 0.87
500	1.69 ± 0.65
1000	1.75 ± 0.55

^aUncertainties were obtained from the standard errors in the fits from each individual trial.

values of ω_0 were obtained from the slopes of the least-square lines and yielded spot size diameters ($2\omega_0$) of $28.3 \pm 2.1 \mu\text{m}$ and $30.3 \pm 0.7 \mu\text{m}$ for 75 and 1000 pulses per spot, respectively. These experimental values agreed well with the spot diameter of $30.2 \mu\text{m}$ measured using silicon as the target.

3.2 Incubation Effects

The results for the accumulated fluence, $N \times \phi_{\text{th}}(N)$, versus incident pulse number, N , are shown in Fig. 4. The data were fit with a power function, and the R^2 value was 0.988. From the equation of the best-fit line, the incubation coefficient, ξ , in Eq. (2) was found to be 0.89 ± 0.03 . From extrapolation, the single-pulse ablation threshold, $\phi_{\text{th}}(1)$, was found to be $3.29 \pm 0.14 \text{ J}/\text{cm}^2$. The incubation coefficient of porcine bone found in our experiments is in the same range as that found for bovine bone.¹⁴ However, the single-pulse ablation threshold with a femtosecond laser source is higher than that found by Lim et al. ($2.70 \pm 0.16 \text{ J}/\text{cm}^2$)¹⁴ using a comparable wavelength and pulse duration.

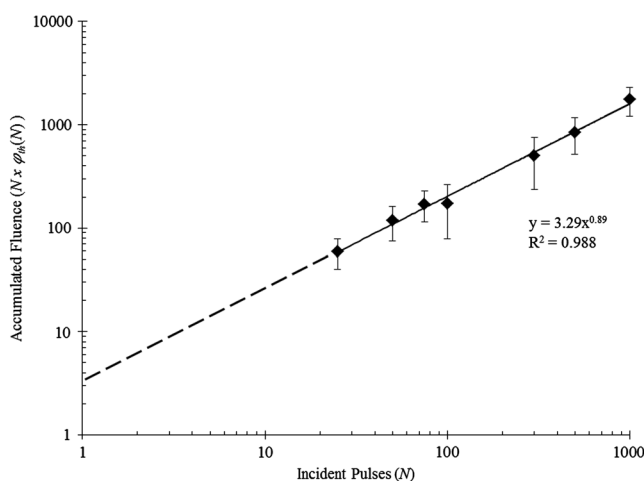


Fig. 4 Incubation power law for porcine cortical bone irradiated with $\lambda = 800 \text{ nm}$ $\tau = 170 \text{ fs}$ pulses. The data were fit with a power function with $R^2 = 0.988$. The incubation coefficient, ξ , was 0.89 ± 0.03 , and the single-pulse ablation threshold fluence was $3.29 \pm 0.14 \text{ J}/\text{cm}^2$.

4 Discussion

The possible use of ultrashort ($<10 \text{ ps}$) lasers in cutting and drilling hard biological tissue has been explored since the 1990s in studies mostly involving dental tissue.^{4,19,20} More recently, studies have investigated the ablation ability and characteristics of ultrashort lasers in cortical bone^{6,14} for the purpose of replacing the mechanical drill and saw used in orthopedic surgery. In these studies, ultrashort pulsed lasers have been shown to result in relatively high rates of tissue removal with minimal thermal damage or mechanical injury—ideal for use in calcified bone since its shear and compressive characteristics make it susceptible to fracture. The ablation threshold has been previously found in porcine cortical bone,⁶ however, it was only investigated at an incident pulse number of 1000. A previous study by Kim et al. using dental tissue showed a decreasing damage threshold with an increasing number of incident pulses.¹⁵ In order to take advantage of the ablation benefits of ultrashort pulsed lasers, the incubation effects in bone must be understood.

In their work on micropillars in bone, Lim et al. characterized the incubation effect in bovine cortical bone.¹⁴ The single-pulse ablation threshold was obtained experimentally, and the 1000-pulse ablation threshold was calculated. However, the calculated 1000-pulse threshold is different from the previous findings of Girard et al. in porcine cortical bone.⁶

Porcine cortical and cancellous bone have been previously shown to best match human bones in their degree of mineralization, composition,²¹ and lamellar structure.²² Unlike previous investigations with bone, the samples in this study were not altered before ablation, which is close to practical surgical conditions. In addition, the use of the scanning electron microscope (SEM) was avoided in this study due to the permanent tissue alterations that would have resulted from the required SEM biological sample preparation.

Figure 2 shows a sample image of ablated craters under $20\times$ microscope viewing. The crater diameter was measured to be the span of the darkened region. The craters appear to have rims of discolored tissue surrounding them. Due to their lightened color, the rims were presumed not to be charred tissue but instead the result of ablation debris or the result of a pressure-driven flow of molten bone tissue from the center to the edge of the crater followed by resolidification at the rim.²³ Some craters were noticeably asymmetrical, which could be the result of surface roughness, heterogeneities in the bone specimens, or the nonideal alignment of optics.

Based on the Gaussian intensity profile approximation, the D^2 method describes a relationship between the diameter of an ablated crater, the material-dependent ablation threshold fluence, the Gaussian beam radius, and the peak fluence of the beam.¹⁷ Figure 3 shows the squared diameter of ablated craters versus the peak laser fluence for incident pulse numbers of 75 and 1000. The slope of the data allows the determination of the effective beam spot size, and an extrapolation of D^2 to intersect with the x axis provides a value for the ablation threshold fluence, $\phi_{\text{th}}(N)$. Since the three trials do not have the same uncertainty, a simple least-squares line fitting all data points would not suffice. Instead, the least-square line was found for each trial (not shown in Fig. 3), and the weighted average slope and intercept were calculated. The resulting fit line was constructed from this average slope and intercept.

As seen in Fig. 3 there appear to be different trends for D^2 through the range of fluence. Above $\sim 2 \text{ J}/\text{cm}^2$, the crater area

appears to increase logarithmically with fluence. At lower fluences, however, the crater area is less deterministic as a function of laser fluence, while a change in ablation mechanism has been reported to occur at a certain fluence in other materials.²⁴ The depths of the craters at fluences $< 2 \text{ J/cm}^2$ were comparable in size to the bone surface irregularities (ridges, pits) and likely do not constitute meaningful tissue removal. Large-scale bone removal or drilling will require greater ablation rates; therefore, this study focused on the characterization of the thresholds of this higher-fluence ablation regime. As a result, our least-square lines were fit using only the data points above 2 J/cm^2 , denoted as solid points in Fig. 3. The irregularities in crater diameter seen in Fig. 3 were likely due to the irregular surface of the sample or the uncertainty in the laser focusing scheme.

The ablation thresholds for different pulse numbers, N , are shown in Table 1. The uncertainties were calculated from the standard deviation in the fit of each individual trial following the weighted-average method for independent measurements. As expected, the ablation threshold decreases as the pulse number increases, from $2.37 \pm 0.78 \text{ J/cm}^2$ with 25 incident pulses to $1.75 \pm 0.55 \text{ J/cm}^2$ at 1000 pulses. After reaching 100 pulses per spot, the accumulation effect appears to saturate. This agrees well with results on ablation of transparent materials from Rosenfeld et al., who found the most dramatic changes in threshold occurred at lower pulse numbers and the reduction in threshold was less pronounced at higher pulse numbers.²⁵ The measured ablation threshold at 1000 pulses differs significantly from that found by Girard et al. with the same number of pulses (0.69 J/cm^2).⁶ One of the likely causes of this discrepancy may be differences in the definition of *ablation*. In the Girard study, ablation was deemed to occur when visual inspection of polished bone SEM images showed laser-induced damage.⁶ In this study, ablation was defined as a definitive removal of tissue and formation of a crater. This measured threshold at 1000 pulses was somewhat greater than the strong ablation threshold found by Lim et al. ($1.22 \pm 0.29 \text{ J/cm}^2$),¹⁴ but there was good agreement at 100 pulses per spot ($1.56 \pm 0.09 \text{ J/cm}^2$). Discrepancies in ablation thresholds found by both Girard et al.⁶ and Lim et al.¹⁴ and those presented in this study are also likely the result of using unaltered bone samples in the current study versus polished bone samples in the other studies.

The reduction in ablation threshold with incident pulse number is referred to as the incubation effect and follows a power law equation¹³ that was originally developed for metals under nanosecond pulse irradiations, but which has been adopted for semiconductors¹² and insulators²⁵ with the use of femtosecond laser pulses. In metals, cumulative effects have been attributed to the accumulation of plastic deformations resulting from thermal stresses caused by incident pulses with fluences below the ablation threshold.²⁶ As a result of these deformations, the metal is then successfully ablated by pulses with laser fluences less than the single-pulse ablation threshold. In the case of semiconductors and insulators, laser-induced alterations such as defects or modifications in chemical properties are believed to be the main reason for incubation effects.^{12,25}

A rearrangement of Eq. (2) yields a double logarithmic relationship between the accumulated fluence, $N \times \phi_{\text{th}}(N)$, and the pulse number, N . The material-dependent incubation coefficient, ξ , is then determined from the log-log plot. The incubation coefficient characterizes the degree of incubation—the change in the ablation threshold with pulse number. A value

of $\xi = 1$ indicates that there is no incubation effect in the material and the ablation threshold will not change with pulse number. As seen in Fig. 4, the porcine cortical bone ablation data fits well with this incubation model. The incubation coefficient was found to be 0.89 ± 0.03 , which agrees very well with the results for the bovine cortical bone incubation coefficient (0.89 ± 0.02).¹⁴ When the incubation data was extrapolated back to $N = 1$ pulses, the single-pulse ablation threshold was found. For porcine cortical bone, it was found to be $3.29 \pm 0.14 \text{ J/cm}^2$. This threshold is marginally higher than the previously found bovine cortical bone single-pulse strong ablation threshold of $2.70 \pm 0.16 \text{ J/cm}^2$.^{2,14} This increase in fluence could be attributed to the rough surface of the bone samples used in this investigation and the difference between bovine and porcine bones. While similar incubation effects occur in porcine and bovine cortical bone, we feel that the greater similarity between the bones of humans and pigs on the microscopic level and the use of unaltered bone allows for the application of the data presented in this study to human subjects.

5 Conclusions

Ultrashort pulsed lasers appear to be ideal for use in orthopedic surgery due to their high ablation efficiency and low collateral damage. Establishing the laser fluence ablation threshold of bone is crucial for understanding the ablation mechanism and for designing clinical ablation protocols. Using the D^2 method, the ablation threshold was determined in unaltered porcine cortical bone at multiple incident pulse numbers ranging from 25 to 1000 pulses per spot. The lowered threshold at greater pulse numbers indicated an incubation effect. Using a power model, the incubation coefficient was found to be 0.89 ± 0.03 , which agreed well with previous results found using bovine tissue. The single-pulse ablation threshold was found to be $3.29 \pm 0.14 \text{ J/cm}^2$, which was higher than the previous findings in bovine bones. The difference in ablation threshold may be attributed to different microstructure and surface topography due to different sample preparation. Unpolished bone specimens were used in our study and are believed to be a better approximation to *in vivo* bone ablation scenarios.

Acknowledgments

The authors would like to acknowledge Mr. Chris Butcher for his technical support at the Canadian Center for Electron Microscopy and the Brockhouse Institute for Material Research, and Drs. Brett Dunlop, Dafydd R. Williams, and Mehran Anvari of St. Joseph's Healthcare Hamilton for valuable discussions. This project was supported in part by the Natural Sciences and Engineering Research Council (NSERC) of Canada, the Canada Foundation for Innovation, and the Ontario Ministry of Research and Innovation.

References

1. C. Gonzalez et al., "Comparison of the erbium-yttrium aluminum garnet and carbon dioxide lasers for *in vitro* bone and cartilage ablation," *Laryngoscope* **100**(1), 14–17 (1990).
2. A. Charlton et al., "Erbium-YAG and holmium-YAG laser ablation of bone," *Laser Med. Sci.* **5**(4), 365–373 (1990).
3. H. Devlin et al., "Healing of bone defects prepared using the erbium-YAG laser," *Laser Med. Sci.* **9**(4), 239–242 (1994).
4. J. Neev et al., "Ultrashort pulse lasers for hard tissue ablation," *IEEE J. Sel. Top. Quant.* **2**(4), 790–800 (1996).

5. W. B. Armstrong et al., "Ultrashort pulse laser ossicular ablation and stapedotomy in cadaveric bone," *Laser Surg. Med.* **30**(3), 216–220 (2002).
6. B. Girard et al., "Effects of femtosecond laser irradiation on osseous tissues," *Laser Surg. Med.* **39**(3), 273–285 (2007).
7. R. G. McCaughey et al., "Femtosecond laser ablation of the stapes," *J. Biomed. Opt.* **14**(2), 024040 (2009).
8. M. Niemz, *Laser-Tissue Interactions: Fundamentals and Applications*, Springer-Verlag, GmbH & Co., Berlin, Heidelberg (1996).
9. K. Ozono and M. Obara, "Tailored ablation processing of advanced biomedical hydroxyapatite by femtosecond laser pulses," *Appl. Phys. A: Mater.* **77**(2), 303–306 (2003).
10. J. Byskov-Neilsen and J.-M. Savolainen, "Ultra-short pulse laser ablation of metals: threshold fluence, incubation coefficient and ablation rates," *Appl. Phys. A: Mater.* **101**(1), 97–101 (2010).
11. P. T. Mannion et al., "The effect of damage accumulation behavior on ablation thresholds and damage morphology in ultrashort laser micro-machining of common metals in air," *Appl. Surf. Sci.* **233**(1–4), 275–287 (2004).
12. J. Bonse et al., "Ultrashort-pulse laser ablation of indium phosphide in air," *Appl. Phys. A: Mater.* **72**(1), 89–94 (2001).
13. Y. Jee, M. F. Becker, and R. M. Walser, "Laser-induced damage on single-crystal metal surfaces," *J. Opt. Soc. Am. B* **5**(3), 648–659 (1988).
14. Y. C. Lim et al., "Micropillar fabrication on bovine cortical bone by direct-write femtosecond laser ablation," *J. Biomed. Opt.* **14**(6), 064021 (2009).
15. B. M. Kim et al., "Effects of high repetition rate and beam size on hard tissue damage due to subpicosecond laser pulses," *Appl. Phys. Lett.* **76**(26), 4001–4003 (2000).
16. A. Borowiec and H. K. Haugen, "Femtosecond laser micromachining of grooves in indium phosphide," *Appl. Phys. A: Mater.* **79**(3), 521–529 (2004).
17. J. M. Liu, "Simple technique for measurements of pulsed Gaussian-beam spot sizes," *Opt. Lett.* **7**(5), 196–198 (1982).
18. D. Ashkenasi et al., "Laser processing of sapphire with picosecond and sub-picosecond pulses," *Appl. Surf. Sci.* **120**(1–2), 65–80 (1997).
19. J. Kruger, W. Kautek, and H. Newesely, "Femtosecond-pulse laser ablation of dental hydroxyapatite and single-crystalline fluoroapatite," *Appl. Phys. A: Mater.* **69**(7), S403–S407 (1999).
20. L. B. Da Silva et al., "Comparison of soft and hard tissue ablation with sub-ps and ns pulse lasers," *Proc. SPIE* **2681**, 196–200 (1996).
21. J. Aerssens et al., "Interspecies differences in bone composition, density, and quality: potential implications for in vivo bone research," *Endocrinology* **139**(2), 663–670 (1998).
22. L. Mosekilde, J. Kragstrup, and A. Richards, "Compressive strength, ash weight, and volume of vertebral trabecular bone in experimental fluorosis in pigs," *Calcif. Tissue Int.* **40**(6), 318–322 (1987).
23. A. Ben-Yakar and R. L. Byer, "Femtosecond laser ablation properties of borosilicate glass," *J. Appl. Phys.* **96**(9), 5316–5323 (2004).
24. S. Nolte et al., "Ablation of metals by ultrashort laser pulses," *J. Opt. Soc. Am. B* **14**(10), 2716–2722 (1997).
25. A. Rosenfeld, M. Lorenz, and D. Ashkenasi, "Ultrashort-laser-pulse damage threshold of transparent materials and the role of incubation," *Appl. Phys. A: Mater.* **69**(7), S373–S376 (1999).
26. C. S. Lee, N. Koumvakalis, and M. Bass, "Spot-size dependence of laser-induced damage to diamond-turned Cu mirrors," *Appl. Phys. Lett.* **41**(7), 625–627 (1982).